

# From Charge to Orbital Ordered Metal-Insulator Transition in Alkaline-Earth Ferrites

Yajun Zhang,<sup>1,2</sup> Michael Marcus Schmitt,<sup>2</sup> Alain Mercy,<sup>2</sup> Jie Wang,<sup>1,\*</sup> and Philippe Ghosez<sup>2,†</sup>

<sup>1</sup>*Department of Engineering Mechanics, School of Aeronautics and Astronautics, Zhejiang University, 38 Zheda Road, Hangzhou 310007, China*

<sup>2</sup>*Theoretical Materials Physics, Q-MAT, CESAM, Université de Liège, Belgium*  
(Dated: March 9, 2024)

While  $\text{CaFeO}_3$  exhibits upon cooling a metal-insulator transition linked to charge ordering,  $\text{SrFeO}_3$  and  $\text{BaFeO}_3$  keep metallic behaviors down to very low temperatures. Moreover, alkaline-earth ferrites do not seem prone to orbital ordering in spite of the  $d^4$  formal occupancy of  $\text{Fe}^{4+}$ . Here, from first-principles simulations, we show that the metal-insulator transition of  $\text{CaFeO}_3$  is structurally triggered by oxygen rotation motions as in rare-earth nickelates. This not only further clarifies why  $\text{SrFeO}_3$  and  $\text{BaFeO}_3$  remain metallic but allows us to predict that an insulating charge-ordered phase can be induced in  $\text{SrFeO}_3$  from appropriate engineering of oxygen rotation motions. Going further, we unveil the possibility to switch from the usual charge-ordered to an orbital-ordered insulating ground state under moderate tensile strain in  $\text{CaFeO}_3$  thin films. We rationalize the competition between charge and orbital orderings, highlighting alternative possible strategies to produce such a change of ground state, also relevant to manganite and nickelate compounds.

ABO<sub>3</sub> perovskite oxides, with a transition metal at the B-site, form a vast class of functional materials, fascinating by the diversity of their unusual properties [1–3]. Amongst them, different families of compounds with a formal  $e_g^1$  occupation of the  $d$  orbitals at the B-site, like rare-earth manganites ( $d^4 = t_{2g}^1 e_g^1$  in  $\text{R}^{3+}\text{Mn}^{3+}\text{O}_3$ , with R a rare-earth element), rare-earth nickelates ( $d^7 = t_{2g}^6 e_g^1$  in  $\text{R}^{3+}\text{Ni}^{3+}\text{O}_3$ ), or alkaline earth ferrites ( $d^4 = t_{2g}^1 e_g^1$  in  $\text{A}^{2+}\text{Fe}^{4+}\text{O}_3$ , with A = Ca, Sr or Ba) are similarly prone to show metal-insulator transitions (MIT). However, the mechanism behind such a transition can be intriguingly different from one family to the other.

$\text{RNiO}_3$  (except  $\text{R}=\text{La}$ ) and  $\text{RMnO}_3$  compounds crystallize in the same metallic  $Pbnm$   $\text{GdFeO}_3$ -type phase at sufficiently high-temperature. This phase is compatible with their small tolerance factor and labeled ( $a^-a^-c^+$ ) in Glazer's notation [4]. It differs from the aristotype cubic perovskite structure, only expected at very high temperature and not experimentally observed, by the coexistence of two types of atomic distortions: (i) in-phase rotation of the oxygen octahedra along  $z$  direction ( $M_z$ ) and (ii) anti-phase tilts of the same oxygen octahedra with identical amplitude around  $x$  and  $y$  directions ( $R_{xy}$ ). On the one hand,  $\text{RNiO}_3$  compounds show on cooling a MIT ( $T_{MIT} = 0 - 600\text{K}$ ) concomitant with a structural transition from  $Pbnm$  to  $P2_1/n$  [5]. This lowering of symmetry arises from the appearance of a breathing distortion of the oxygen octahedra ( $B_{oc}$ ), recently assigned to a structurally triggered mechanism [6] and producing a kind of charge ordering (CO) [7–10]. On the other hand,  $\text{RMnO}_3$  compounds also exhibit on cooling a MIT ( $T_{MIT} \approx 750\text{K}$ ) but associated to orbital ordering (OO) and linked to the appearance of Jahn-Teller distortions ( $M_{JT}$ ) compatible with the  $Pbnm$  symmetry [11, 12].

In comparison,  $\text{AFeO}_3$  compounds do not behave so systemically and adopt seemingly different behaviors. While  $\text{SrFeO}_3$  and  $\text{BaFeO}_3$  keep the ideal cubic per-

ovskite structure and show metallic behavior at all temperatures [13, 14],  $\text{CaFeO}_3$ , which crystallizes above room temperature in a  $Pbnm$   $\text{GdFeO}_3$ -type phase, exhibits a behavior similar to nickelates. At 290K, a MIT takes place at the same time as its symmetry is lowered to  $P2_1/n$  due to the appearance of a breathing distortion [15, 16]. A variety of explanations have been previously proposed to elucidate the MIT in  $\text{CaFeO}_3$ , including orbital hybridization [17], electron-lattice interactions [18, 19], and ferromagnetic coupling [20]. However, no net picture has emerged yet to rationalize its behavior and that of other ferrites.

Here, we show from first-principles calculations that the CO-type MIT in bulk  $\text{CaFeO}_3$  arises from the same microscopic mechanism as in the nickelates and must be assigned to a progressive triggering of  $B_{oc}$  atomic distortions by  $M_z$  and  $R_{xy}$  atomic motions. We demonstrate that this triggered mechanism is universal amongst the ferrite family and that an insulating phase can be induced in metallic  $\text{SrFeO}_3$  from appropriate tuning of oxygen rotations and tilts. Going further, we reveal that CO and OO compete in  $\text{AFeO}_3$  compounds and we unveil the possibility to switch from CO-type to OO-type MIT in  $\text{CaFeO}_3$  thin films under appropriate strain conditions. This offers a convincing explanation for the enormous resistivity at room-temperature recently found in  $\text{CaFeO}_3$  films grown on  $\text{SrTiO}_3$  [21].

**Methods** - Our first-principles calculations relied on density functional theory (DFT) as implemented in VASP [22, 23]. We worked with the PBEsol [24] exchange-correlation functional including U and J corrections as proposed by Liechtenstein [25]. We used  $(U|J) = (7.2|2.0)\text{eV}$ , a plane-wave energy cutoff of  $600\text{eV}$  and Monkhorst-Pack [26] k-point samplings equivalent to  $12 \times 12 \times 12$  for a 5-atoms cubic perovskite cell. The lattice parameters and internal atomic coordinates were relaxed until atomic forces are less than  $10^{-5}\text{eV}/\text{\AA}$ . The

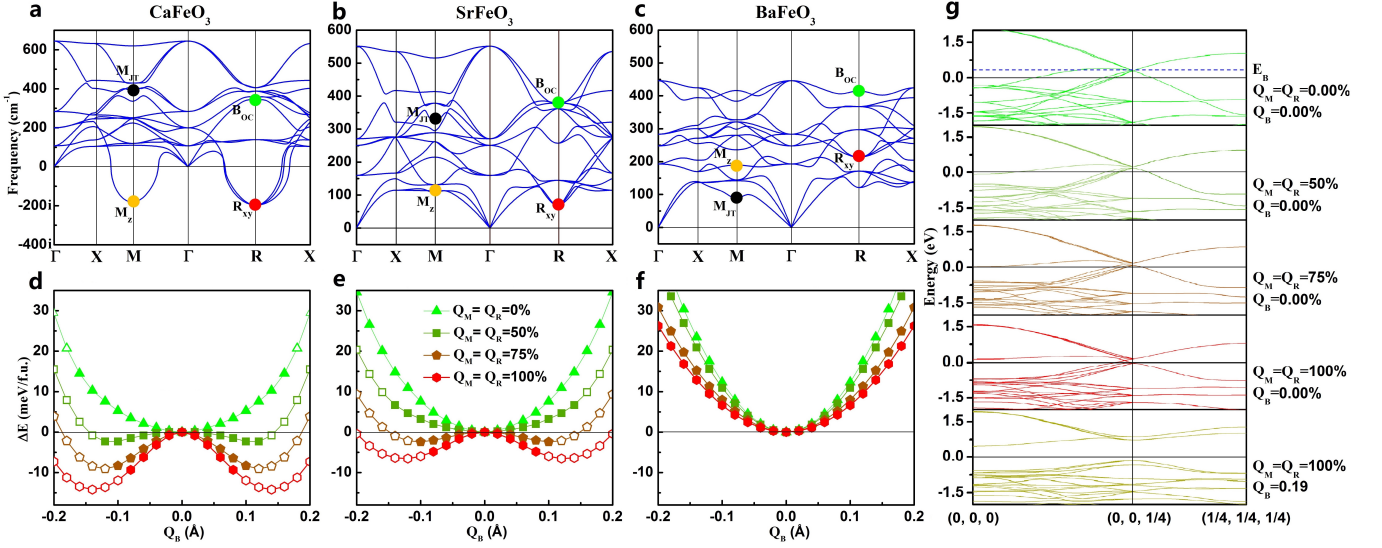


FIG. 1: (a-c) Phonon dispersion curves of cubic  $\text{CaFeO}_3$  (a),  $\text{SrFeO}_3$  (b), and  $\text{BaFeO}_3$  (c) on which most relevant modes are pointed. (d-f) Evolution of the energy with respect to the breathing distortion ( $Q_B$ ) at fixed rotation ( $Q_M$ ) and tilts ( $Q_R$ ) amplitudes in  $\text{CaFeO}_3$  (d),  $\text{SrFeO}_3$  (e), and  $\text{BaFeO}_3$  (f). Opened (resp. filled) symbols denote insulating (resp. metallic) states. (g) Electronic band structure of  $\text{CaFeO}_3$  along selected lines of the  $Pbnm$  or  $P2_1/n$  Brillouin zone (coordinates in pseudo-cubic notations) for different amplitude of distortions. All results were calculated with FM spin order and using a fixed cubic cell with the same volume as the ground state. Distortion amplitudes are normalized to those calculated by *ISODISTORT*[27] in the  $\text{CaFeO}_3$  AFM ground state.

phonon dispersion curves were calculated with  $2 \times 2 \times 2$  supercells using finite displacement method. A special care was devoted to the determination of appropriate  $U$  and  $J$  parameters, which is discussed in detail in the Supplementary Material (SM) [35]. We found that  $(U|J) = (7.2|2.0)$  eV provides good simultaneous description of the structural (lattice constant and distortion amplitudes), electronic (insulating ground-state) and magnetic (AFM spiral-type ground state very close in energy to the FM configuration) properties of  $\text{CaFeO}_3$ .

**Bulk  $\text{CaFeO}_3$**  – In order to clarify the mechanism behind the  $P2_1/n$  insulating ground state of  $\text{CaFeO}_3$ , we first focus on the phonon dispersion curves of its parent cubic phase (Fig. 1a). Calculations are reported in a ferromagnetic configuration, which is representative to unravel the essential physics. On the one hand, Fig. 1a shows expected unstable phonon modes at M point ( $M_2^+$ ,  $\omega_M = 181 \text{ i cm}^{-1}$ ) and R point ( $R_5^-$ ,  $\omega_R = 197 \text{ i cm}^{-1}$ ) of the Brillouin zone, related respectively to the  $M_z$  and  $R_{xy}$  distortions yielding the  $Pbnm$  phase. On the other hand, it attests that the  $R_2^-$  mode related to the  $B_{oc}$  distortion is significantly stable ( $\omega_B^- = 343 \text{ cm}^{-1}$ ), so questioning the origin of its appearance in the  $P2_1/n$  phase.

The answer is provided in Fig. 1b), reporting the evolution of the energy with the amplitude of  $B_{oc}$  ( $Q_B$ ) at fixed amplitudes of  $M_z$  ( $Q_M$ ) and  $R_{xy}$  ( $Q_R$ ). It demonstrates that, although initially stable (single well – SW – with a positive curvature at the origin  $\alpha_B \propto \omega_B^2 > 0$ ) in the cubic phase,  $B_{oc}$  will be progressively destabilized (double well – DW – with a renormalized negative curva-

ture at the origin  $\tilde{\alpha}_B < 0$ ) as  $M_z$  and  $R_{xy}$  develop in the  $Pbnm$  phase. The curvature  $\tilde{\alpha}_B$  changes linearly with  $Q_M^2$  and  $Q_R^2$  ( $\tilde{\alpha}_B = \alpha_B + \lambda_{BM}Q_M^2 + \lambda_{BR}Q_R^2$ ) so that its evolution must be assigned to a *cooperative* biquadratic coupling ( $\lambda_{BM}, \lambda_{BR} < 0$ ) of  $B_{oc}$  with  $M_z$  and  $R_{xy}$  as highlighted by the following terms in the Landau-type energy expansion around the cubic phase:

$$E \propto \alpha_B Q_B^2 + \lambda_{BM} Q_M^2 Q_B^2 + \lambda_{BR} Q_R^2 Q_B^2 \quad (1)$$

For large enough amplitudes of  $M_z$  and  $R_{xy}$ ,  $B_{oc}$  becomes unstable and will spontaneously appear in the structure. In Fig. 1b) we further notice that the amplitude of  $B_{oc}$  required for making the system insulating decreases for increasing  $M_z$  and  $R_{xy}$ , yielding therefore an insulating  $P2_1/n$  ground state.

This behavior is point by point similar to that reported recently in rare-earth nickelates by Mercy *et al.*[6] who subsequently assigned the MIT to a structurally triggered phase transition, in the sense originally defined by Holakovský [28]. In Ref. [6], the unusual cooperative coupling of  $B_{oc}$  with  $M_z$  and  $R_{xy}$  at the origin of this triggered mechanism was moreover traced back in the electronic properties of nickelates and further related to a type of structurally triggered Peierls instability.

Fig 1g) shows that this explanation still holds for ferrites. In the cubic phase of  $\text{CaFeO}_3$  ( $\text{Fe}^{4+}$  with formal occupation  $d^4 = t_{2g}^1 e_g^3$ ), the Fermi energy,  $E_F$ , crosses anti-bonding Fe  $3d$  – O  $2p$  states with a dominant  $e_g$  character. Activation of  $B_{oc}$  can open a gap in these partly occupied  $e_g$  bands at  $q_B = (1/4, 1/4, 1/4)$ , but around an

energy  $E_B$  initially above  $E_F$ . The role of  $R_{xy}$  and  $M_z$  is to tune Fe  $3d$  – O  $2p$  hybridizations in such a way that  $E_B$  is progressively lowered towards  $E_F$ . As they develop into the structure, activating  $B_{oc}$  affects more and more substantially energy states around  $E_F$  and yields an increasing gain of electronic energy explaining the progressive softening of  $\omega_B$ . The  $e_g$  bandwidth in  $\text{CaFeO}_3$  being smaller than in the nickelates,  $E_B$  is initially closer to  $E_F$  consistently with a softer  $\omega_B$  and the smaller amplitude of  $R_{xy}$  and  $M_z$  required to destabilize  $B_{oc}$ .

**Bulk  $\text{SrFeO}_3$  and  $\text{BaFeO}_3$**  – The triggered mechanism highlighted above further straightforwardly explains the absence of MIT in other alkaline-earth ferrites. Because of their larger tolerance factors and as confirmed from the absence of unstable mode in their phonon dispersion curves (Fig. 1b) and c))  $\text{SrFeO}_3$  and  $\text{BaFeO}_3$  preserve their cubic structure down to zero Kelvin [13, 14] and so do not spontaneously develop the oxygen rotation and tilts mandatory to trigger the MIT. The cooperative coupling of  $B_{oc}$  with  $M_z$  and  $R_{xy}$  remains however a generic features of all ferrite compounds.

As illustrated in Fig. 1e) and 1f),  $B_{oc}$  is progressively destabilized when increasing artificially the amplitudes of  $M_z$  and  $R_{xy}$  distortions in  $\text{SrFeO}_3$  and  $\text{BaFeO}_3$ . Since, in the cubic phase of these compounds,  $\omega_B$  is originally at frequencies slightly larger than in  $\text{CaFeO}_3$  ( $\omega_B = 362\text{cm}^{-1}$  in  $\text{SrFeO}_3$  and  $\omega_B = 415\text{cm}^{-1}$  in  $\text{BaFeO}_3$ ), larger distortions are required to induce the MIT. In  $\text{SrFeO}_3$ , amplitudes of  $M_z$  and  $R_{xy}$  corresponding to 75% of their ground-state values in  $\text{CaFeO}_3$  are nevertheless enough to force an insulating ground state. In  $\text{BaFeO}_3$ , the cooperative coupling is less efficient and much larger amplitudes would be required.

This highlights the possibility of inducing a MIT in  $\text{SrFeO}_3$  thin films or heterostructures under appropriate engineering of  $R_{xy}$  and  $M_z$ . Moreover, it provides a vivid explanation to the decrease of  $T_{MIT}$  experimentally observed in  $\text{Ca}_{1-x}\text{Sr}_x\text{FeO}_3$  solid solutions as  $x$  increases [29]. For increasing Sr concentrations, the average tolerance factor increases and the mean amplitudes of  $M_z$  and  $R_{xy}$  decrease. This analysis is supported by DFT calculation at 50/50 Ca/Sr composition using an ordered supercell (see SM [35]).

**Charge versus orbital ordering** – It remains intriguing why  $\text{CaFeO}_3$  ( $t_{2g}^3 e_g^1$ ) prefers to exhibit a breathing distortion ( $B_{oc}$ ) and CO as  $\text{RNiO}_3$  compounds ( $t_{2g}^6 e_g^1$ ) rather than a Jahn-Teller distortion ( $M_{JT}$ ) and OO as  $\text{RMnO}_3$  compounds ( $t_{2g}^3 e_g^1$ ). In Ref. [30] Whangbo *et al.* argue that  $B_{oc}$  is favored in  $\text{CaFeO}_3$  by the relatively strong covalent character of the Fe-O bond while the  $M_{JT}$  distortion is preferred in  $\text{LaMnO}_3$  by the weak covalent character of the Mn-O bond. So, we anticipate that weakening the covalence by increasing the Fe-O distance might favor  $M_{JT}$  and OO in  $\text{CaFeO}_3$ . To realize practically this idea, we investigated the role of tensile epitaxial strain on the ground state of  $\text{CaFeO}_3$  thin films.

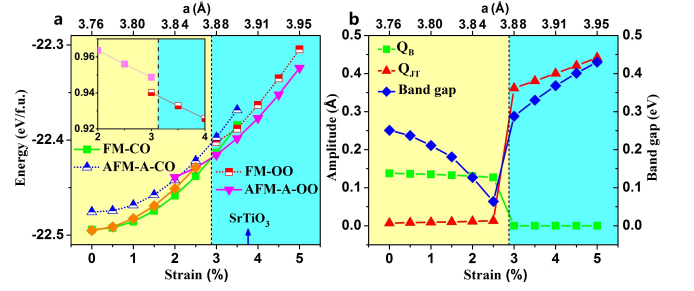


FIG. 2: (a) Total energy as a function of tensile strain (or in-plane lattice constant) for  $\text{CaFeO}_3$  epitaxial films with c-axis out-of-plane, in CO and OO states with either FM or A-type AFM spin ordering; FM CO state with the long c-axis in-plane is plot in orange for comparison. A change of ground state from FM-CO phase (yellow area) to A-type AFM-OO phase (blue area) is observed. Inset:  $c/a$  ratio of the ground state structure as a function of strain. (b) Evolution of  $Q_B$  (green),  $Q_{JT}$  (red) and band gap (blue) as a function of strain (or in-plane lattice constant).

**$\text{CaFeO}_3$  thin films** – The phase diagram of  $\text{CaFeO}_3$  films epitaxially grown on a cubic perovskite (001)-substrate is reported Fig. 2a). The evolution of the energy with the lattice constant of the substrate is shown for FM and A-type AFM orders with either charge or orbital ordering. Although S- and T-type spiral magnetic orders (not shown here) possess a slightly lower energy at the bulk level, the FM order becomes quickly the GS under small tensile strain; C-type and G-type AFM order are much higher in energy and not shown. Both possible orientations of the orthorhombic ( $a^-a^-c^+$ ) oxygen rotation pattern, with the long c-axis either in-plane or out-of-plane were also considered: while c-axis in-plane is favored at zero strain, c-axis out-of-plane becomes more stable under tensile strains.

Fig. 2a) demonstrates the possibility of switching from a CO to an OO ground state in  $\text{CaFeO}_3$  using strain engineering: under increasing tensile strain, the ground state of the film changes from an insulating FM-CO  $P2_1/n$  configuration at small strain to an insulating A-type AFM-OO  $Pbnm$  configuration above 3% tensile strain ( $a=3.88\text{\AA}$ ). Fig. 2b) highlights the strain evolution of  $B_{oc}$  and  $M_{JT}$  distortions together with the change of band gap. Under increasing tensile strain,  $B_{oc}$  slightly decreases and is abruptly suppressed at the phase transition; at the same time, the band gap – already reduced in this FM phase – decreases, although much faster than  $B_{oc}$  and the transition appears precisely when the bandgap converges to zero. Conversely,  $M_{JT}$  is nearly zero below 3% tensile strain while it suddenly appears at the transition and then continuously increases. Amazingly, the amplitude of  $M_{JT}$  ( $0.37\text{\AA}$ ) in a  $\text{CaFeO}_3$  film grown on a  $\text{SrTiO}_3$  substrate ( $a = 3.905\text{\AA}$ ) is comparable to that of bulk  $\text{LaMnO}_3$  ( $0.36\text{\AA}$ ). Such similar amplitude suggests that the  $T_{MIT}$  associated to the OO state in strained

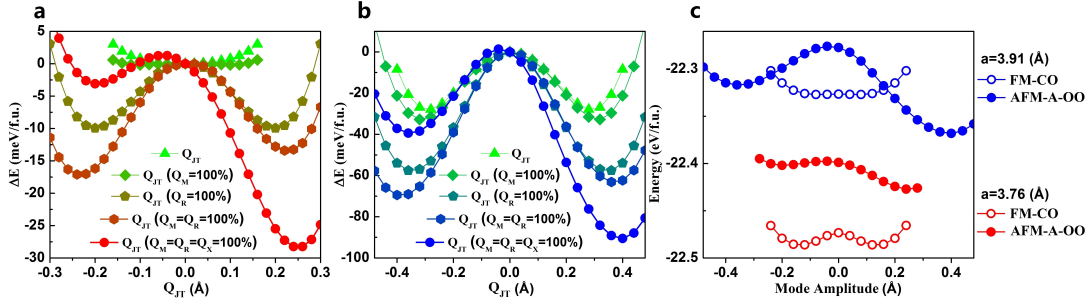


FIG. 3: Evolution of the energy with Jahn-Teller distortion amplitude  $Q_{JT}$  in AFM-A magnetic order and at fixed amplitudes of other distortion (see legend) for  $\text{CaFeO}_3$  epitaxial films under strain of (a) 0% ( $a = 3.76 \text{ \AA}$ ) and (b) 4% ( $a = 3.91 \text{ \AA}$ ). (c) Evolution of the total energy as a function of  $Q_B$  in FM-CO state (open symbol) and  $Q_{JT}$  in A-type AFM-OO state (filled symbol) for  $\text{CaFeO}_3$  thin film under 0% ( $a = 3.76 \text{ \AA}$ , red) and 4% ( $a = 3.91 \text{ \AA}$ , blue) strains.  $Q_M$ ,  $Q_R$  and  $Q_X$  are fixed to their amplitudes in the relevant phase (except for the FM-CO state at 4% which cannot be stabilized and for which we kept positions in the A-type AFM-OO phase).

TABLE I: Top: Amplitudes of dominant distortions [27] in the relaxed CO (FM) and OO (AFM-A) phases of  $\text{CaFeO}_3$  epitaxial films under 0% ( $a = 3.76 \text{ \AA}$ ) and 4% ( $a = 3.91 \text{ \AA}$ ) tensile strain. Bottom : Energy contributions associated to the different terms in Eq.(2), obtained from the amplitudes of distortion reported above.

Amplitudes ( $\text{\AA}$ )	$Q_{JT}$	$Q_B$	$Q_M$	$Q_R$	$Q_X$
$a = 3.76 \text{ \AA}$ -CO	0.007	0.137	0.788	1.111	0.440
$a = 3.76 \text{ \AA}$ -OO	0.256	0.000	0.717	1.194	0.457
$a = 3.91 \text{ \AA}$ -OO	0.400	0.000	0.676	1.309	0.552
Energies (meV/fu)	$\Delta E_{JT}^{(1)}$	$\Delta E_{JT}^{(2)}$	$\Delta E_{JT}^{(3)}$	$\Delta E_{JT}$	$\Delta E_{AFM-A}$
$a = 3.76 \text{ \AA}$ -OO	4.4	-43.6	-15.8	-55.0	74.5
$a = 3.91 \text{ \AA}$ -OO	-104.3	-80.9	-31.0	-216.2	49.3

$\text{CaFeO}_3$  films might be much larger than the  $T_{MIT}$  associated to the CO state in bulk and comparable to the one of  $\text{LaMnO}_3$  ( $T_{MIT} = 750 \text{ K}$ ).

Our findings provide a convincing explanation for the insulating character of  $\text{CaFeO}_3$  films on  $\text{SrTiO}_3$  at room temperature and for the absence of CO MIT in the 100-300K temperature range as recently pointed out in Ref.[21]. They suggest to probe the presence of OO MIT at higher temperature. A key feature, highlighted in the insert in Fig. 2a), is the jump of  $c/a$  ratio at the transition boundary, which provides another concrete hint for experimentalists to probe the CO-OO transition.

*Competition between charge and orbital orders* - To rationalize the emergence of an OO ground state in  $\text{CaFeO}_3$  films, we quantify the lowest-order couplings of  $M_{JT}$  with other distortions in a Landau-type free energy expansion and investigate their sensitivity to magnetic order and epitaxial strain :

$$E \propto \alpha_{JT} Q_{JT}^2 + \lambda_{MJ} Q_M^2 Q_{JT}^2 + \lambda_{RJ} Q_R^2 Q_{JT}^2 + \gamma Q_R Q_X Q_{JT} \quad (2)$$

The first term quantifies the *proper* harmonic energy contribution  $\Delta E_{JT}^{(1)}$  associated to the appearance of  $M_{JT}$ . The second and third terms in Eq. (2) account for a change of energy  $\Delta E_{JT}^{(2)}$  in presence of  $M_z$  and  $R_{xy}$ , linked to their lowest bi-quadratic coupling with  $M_{JT}$ . Finally, sizable anti-polar motions of the Ca cations and apical oxygens ( $X_{AP}$  mode of amplitude  $Q_X$ , see Table I), which are driven by  $M_z$  and  $R_{xy}$ [31], couple in a trilinear term with  $R_{xy}$  and  $M_{JT}$  (last term in Eq.(2)). This coupling produces an energy lowering  $\Delta E_{JT}^{(3)} < 0$ , through a so-called *hybrid improper* mechanism yielding an asymmetry in the  $M_{JT}$  energy well [36]. Compensiously, appearance of a  $M_{JT}$  distortion requires  $\Delta E_{JT} = \Delta E_{JT}^{(1)} + \Delta E_{JT}^{(2)} + \Delta E_{JT}^{(3)} < 0$ .

In bulk  $\text{CaFeO}_3$ ,  $\alpha_{JT}$  is large ( $\omega_{JT}(\text{FM}) = 390 \text{ cm}^{-1}$ ) in the FM cubic phase, which prohibits  $\Delta E_{JT}$  to become negative for sizable amplitudes of  $M_{JT}$ . Switching to the A-type AFM spin order tremendously lowers  $\alpha_{JT}$  ( $\omega_{JT}(\text{AFM} - A) = 144 \text{ cm}^{-1}$ ) but simultaneously increases the total energy by  $\Delta E_{AFM-A}$ . The stabilization of an OO phase with  $M_{JT}$  against the CO phase with  $B_{oc}$  so depends eventually on the counterbalance between  $\Delta E_{AFM-A}$  and  $\Delta E_{JT}$ .

This is quantified for epitaxial thin films in Fig. 3 and Table I. Under negligible tensile strain ( $a = 3.76 \text{ \AA}$ , Fig. 3a), with A-type AFM order,  $\omega_{JT}$  is even softer than in bulk  $\text{CaFeO}_3$ , yielding  $\Delta E_{JT}^{(1)} \approx 0$ . Then, similarly to what was discussed for  $B_{oc}$  in bulk compounds,  $R_{xy}$  and  $M_z$  trigger  $M_{JT}$  ( $\lambda_{MJ}, \lambda_{RJ} < 0$ ), yielding  $\Delta E_{JT}^{(2)} < 0$ . Finally, the hybrid improper coupling with  $X_{AP}$  and  $R_{xy}$  provides a further  $\Delta E_{JT}^{(3)} < 0$ . However, although globally negative,  $\Delta E_{JT}$  cannot overcome  $\Delta E_{AFM-A}$  (Fig. 3c). Under large tensile strain ( $a = 3.91 \text{ \AA}$ , Fig. 3b)  $\alpha_{JT}$  is significantly reduced by coupling with the epitaxial tetragonal strain  $e_{tz}$  ( $\alpha_{JT} \propto \gamma_{tj} e_{tz} + \lambda_{tj} e_{tz}^2$  [32]), yielding a huge negative  $\Delta E_{JT}^{(1)}$ . Then, although  $\lambda_{MJ}$  and  $\lambda_{RJ}$  are reduced and  $\gamma$  remains unaffected (see SM



[35]),  $\Delta E_{JT}^{(2)}$  and  $\Delta E_{JT}^{(3)}$  are increased roughly by a factor of 2, mainly due to the increase of  $Q_{JT}$ . Globally,  $|\Delta E_{JT}|$  in A-type AFM order is now much larger than  $\Delta E_{AFM-A}$ , which moreover has been slightly reduced, and the OO phase with  $M_{JT}$  is stabilized against the CO phase with  $B_{oc}$  (Fig. 3c). We notice that  $Q_M$  and  $Q_R$  are not strongly affected by strain so that the stabilization of the OO phase must be primarily assigned to the strain remormalization of  $\alpha_{JT}$ .  $E_{JT}^{(2)}$  and  $\Delta E_{JT}^{(3)}$  play however an important complementary role and tuning  $Q_M$  and  $Q_R$  would offer an alternative strategy to stabilize the OO phase.

**Conclusions** - We have rationalized the appearance of a CO-type MIT in alkaline-earth ferrites, showing that, in  $\text{CaFeO}_3$ , such a MIT arises from the triggering of  $B_{oc}$  by  $M_z$  and  $R_{xy}$  and that this mechanism can induce a CO insulating ground state in  $\text{SrFeO}_3$  under appropriate tuning of  $M_z$  and  $R_{xy}$ . Going further, we found that OO is also incipient to  $\text{CaFeO}_3$  and that an OO-type MIT can be engineered in thin films under moderate tensile strain. We have shown that the appearance of the OO-type insulating ground state arises from a delicate balance between different energy terms, suggesting different strategies to stabilize it. Interestingly, the emergence of the OO phase in ferrites is the result of a purely structural instability and we did not find any gradient discontinuity in the energy (corner point), fingerprint of the electronic instability usually associated to OO phases[33]. Such a structural stabilization of the OO phase might offer a reasonable explanation to the emergence of an OO phase in other materials like  $\text{RNiO}_3$  compounds [34][37].

**Acknowledgments** - Work supported by the FRS-FNRS PDR project HiT4FiT and ARC AIMED. M.S. and Y. Z. acknowledge financial support from FRIA (grants 1.E.070.17. and 1.E.122.18.). Computational support from Cécili funded by F.R.S-FNRS (Grant No. 2.5020.1) and Tier-1 supercomputer of the Fédération Wallonie-Bruxelles funded by the Walloon Region (Grant No. 1117545). M.S. and Y.Z. contributed equally to this work.

---

\* Electronic address: [jw@zju.edu.cn](mailto:jw@zju.edu.cn)

† Electronic address: [Philippe.Ghosez@ulg.ac.be](mailto:Philippe.Ghosez@ulg.ac.be)

- [1] D. Khomskii, *Transition metal compounds* (Cambridge University Press, 2014).
- [2] M. Imada, A. Fujimori, and Y. Tokura, *Rev. Mod. Phys.* **70**, 1039 (1998).
- [3] P. Zubko, S. Gariglio, M. Gabay, P. Ghosez, and J.-M. Triscone, *Annu. Rev. Condens. Ma. P.* **2**, 141 (2011), <https://doi.org/10.1146/annurev-conmatphys-062910-140445>.
- [4] A. M. Glazer, *Acta Crystallogr. B.* **28**, 3384 (1972).
- [5] M. L. Medarde, *J. Phys.: Condens. Matter* **9**, 1679 (1997).
- [6] A. Mercy, J. Bieder, J. Iñiguez, and P. Ghosez, *Nat.*

*Commun.* **8**, 1677 (2017).

- [7] I. I. Mazin *et al.* *Phys. Rev. Lett.* **98**, 176406 (2007).
- [8] H. Park, A. J. Millis, and C. A. Marianetti, *Phys. Rev. Lett.* **109**, 156402 (2012).
- [9] S. Johnston, A. Mukherjee, I. Elfimov, M. Berciu, and G. A. Sawatzky, *Phys. Rev. Lett.* **112**, 106404 (2014).
- [10] J. Varignon, M. N. Grisolia, J. Iñiguez, A. Barthélémy, and M. Bibes, *npj Quantum Materials* **2**, 21 (2017).
- [11] T. Kimura, S. Ishihara, H. Shintani, T. Arima, K. T. Takahashi, K. Ishizaka, and Y. Tokura, *Phys. Rev. B* **68**, 060403 (2003).
- [12] M. C. Sánchez, G. Subías, J. García, and J. Blasco, *Phys. Rev. Lett.* **90**, 045503 (2003).
- [13] J. B. MacChesney, R. C. Sherwood, and J. F. Potter, *J. Chem. Phys.* **43**, 1907 (1965).
- [14] N. Hayashi *et al.* *Angew. Chem. Int. Edit.* **50**, 12547 (2011).
- [15] S. Kawasaki, M. Takano, R. Kanno, T. Takeda, and A. Fujimori, *J. Phys. Soc. Jpn.* **67**, 1529 (1998).
- [16] P. M. Woodward, D. E. Cox, E. Moshopoulou, A. W. Sleight, and S. Morimoto, *Phys. Rev. B* **62**, 844 (2000).
- [17] T. Akao *et al.* *Phys. Rev. Lett.* **91**, 156405 (2003).
- [18] J. Matsuno, T. Mizokawa, A. Fujimori, Y. Takeda, S. Kawasaki, and M. Takano, *Phys. Rev. B* **66**, 193103 (2002).
- [19] S. Ghosh *et al.*, *Phys. Rev. B* **71**, 245110 (2005).
- [20] A. Cammarata and J. M. Rondinelli, *Phys. Rev. B* **86**, 195144 (2012).
- [21] P. C. Rogge *et al.*, *Phys. Rev. Materials* **2**, 015002 (2018).
- [22] G. Kresse and J. Hafner, *Phys. Rev. B* **47**, 558 (1993).
- [23] P. E. Blöchl, *Phys. Rev. B* **50**, 17953 (1994).
- [24] J. P. Perdew, A. Ruzsinszky, G. I. Csonka, O. A. Vydrov, G. E. Scuseria, L. A. Constantin, X. Zhou, and K. Burke, *Phys. Rev. Lett.* **100**, 136406 (2008).
- [25] V. I. Anisimov, F. Aryasetiawan, and A. I. et Lichtenstein, *J. Phys.: Condens. Matter* **9**, 767 (1997).
- [26] H. J. Monkhorst and J. D. Pack, *Phys. Rev. B* **13**, 5188 (1976).
- [27] B. J. Campbell, H. T. Stokes, D. E. Tanner, and D. M. Hatch, *J. Appl. Crystallogr.* **39**, 607 (2006).
- [28] J. Holakovský, *physica status solidi (b)* **56**, 615 (1973).
- [29] T. Takeda, R. Kanno, Y. Kawamoto, M. Takano, S. Kawasaki, T. Kamiyama, and F. Izumi, *Solid State Sci.* **2**, 673 (2000).
- [30] M.-H. Whangbo, H.-J. Koo, A. Villesuzanne, and M. Pouchard, *Inorg. Chem.* **41**, 1920 (2002), pMID: 11925189, <https://doi.org/10.1021/ic0110427>.
- [31] J. Varignon, N. C. Bristowe, E. Bousquet, and P. Ghosez, *Sci. Rep.* **5**, 15364 (2015).
- [32] M. A. Carpenter and C. J. Howard, *Acta Crystallogr. B.* **65**, 134 (2009).
- [33] W.-G. Yin, D. Volja, and W. Ku, *Phys. Rev. Lett.* **96**, 116405 (2006).
- [34] Z. He and A. J. Millis, *Phys. Rev. B* **91**, 195138 (2015).
- [35] See supplementary material at [URL](#) for details about the determination of (U|J) calculation parameters, supporting calculations on  $\text{Sr/BeFeO}_3$  solutions, and a deeper analysis on the asymmetry of the  $Q_{JT}$  energy surface.
- [36] The coexistence of  $M_z$  and  $R_{xy}$  already produces an asymmetry in the energy well through the term  $E \propto \delta Q_R^2 Q_M Q_{JT}$ . However, this asymmetry is in the negligible range of 1 meV (see Fig. 3a-b), and is not further discussed here.
- [37] Xu He *et al.*, in press.